CONDENSED MATTER PHYSICS

Nontrivial quantum oscillation geometric phase shift in a trivial band

Biswajit Datta[1]*, Pratap Chandra Adak[1], Li-kun Shi[2], Kenji Watanabe[3], Takashi Taniguchi[3], Justin C. W. Song[2,4]*, Mandar M. Deshmukh[1]*

Quantum oscillations provide a notable visualization of the Fermi surface of metals, including associated geometrical phases such as Berry's phase, that play a central role in topological quantum materials. Here we report the existence of a new quantum oscillation phase shift in a multiband system. In particular, we study the ABA-trilayer graphene, the band structure of which is composed of a weakly gapped linear Dirac band, nested within a quadratic band. We observe that Shubnikov-de Haas (SdH) oscillations of the quadratic band are shifted by a phase that sharply departs from the expected 2π Berry's phase and is inherited from the nontrivial Berry's phase of the linear band. We find this arises due to an unusual filling enforced constraint between the quadratic band and linear band Fermi surfaces. Our work indicates how additional bands can be exploited to tease out the effect of often subtle quantum mechanical geometric phases.

INTRODUCTION

The accumulation of a nontrivial geometric phase in quantum oscillations of a band is often a telltale sign of a rich underlying internal structure (1–4). These can arise from diverse settings, including strong spin-orbit coupled systems that have real-space (5, 6) or momentum-space spin texture (7), periodic driving by strong electromagnetic fields (8), and multiorbital/site structure within a unit cell (9). Although these phases are often encoded in the subtle twisting of electronic wave functions, their impact on material response can be profound, being responsible for a wealth of unusual quantum behaviors that include unconventional magnetoelectric coupling (10), an emergent electromagnetic field for electrons (6), and protected edge modes (11) among others.

A prominent example is the Berry's phase (12–14). In anomalous Hall metals, the Berry's phase on the Fermi surface determines the (unquantized part of the) anomalous Hall conductivity (15, 16); nontrivial π Berry's phase enforces the absence of backscattering in topological materials (17). The value of the Berry's phase of electrons as they encircle a single, closed Fermi surface can be used as a litmus test for topological bands: π indicates a nontrivial band (18–22), whereas 2π indicates a massive quadratic band (23–25). In the presence of a magnetic field (B), the (quantized) size of closed cyclotron orbits depends on both the magnetic flux threading the orbits and the Berry's phase of electrons. As a result, quantum oscillations of a closed Fermi surface can acquire phase shifts—a direct result of the Berry's phase of electrons (3). This is visible in oscillations of both resistance and thermodynamic quantities like magnetization. Tracking these quantum oscillation phase shifts has emerged as a powerful probe for topological materials (26–30).

RESULTS

Here, we unveil a new phase shift for quantum oscillations that appears in multi–Fermi surface metals. In particular, we reveal how

the quantum oscillations of a massive quadratic band (with a constant and trivial Berry's phase) can acquire nontrivial ($\pm\pi$) phase shifts that are gate tunable. The unusual phase shifts are found in measured Shubnikov–de Haas (SdH) oscillations of a quadratic band in a multiband system—the ABA-trilayer graphene. The phase shift of the quadratic band SdH oscillations depends on the position of the Fermi level in the coexisting Dirac band. The phase switches sharply from π to $-\pi$ as the Fermi level is tuned from below the Dirac bandgap to
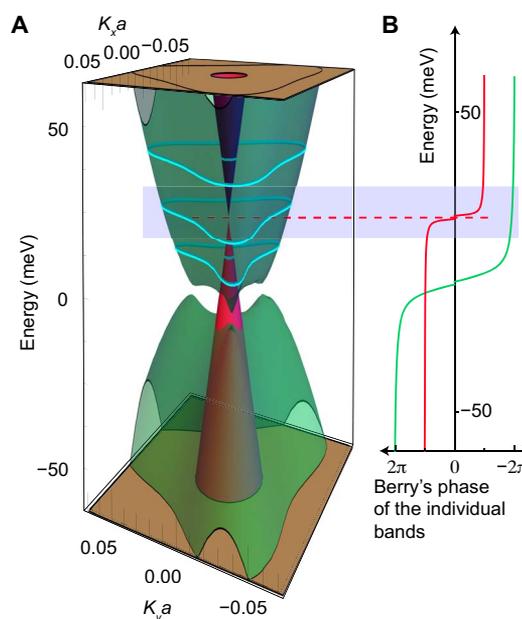

Fig. 1. Band diagram of the ABA-trilayer graphene. (A) Band diagram of the ABA-stacked trilayer graphene showing one pair of the conical band (colored red) and another pair of the quadratic band (colored green). The Fermi surface at three different energies is overlaid for which the Fermi energy lies in the valence band, in the bandgap, and in the conduction band of the MLG-like band. There is no contour from the MLG-like band when Fermi energy is in the bandgap. (B) Calculated Berry's phase plot with same color codes for both bands. Since the bands are gapped, the Berry's phase of the individual bands goes to zero at the respective band edges. The shaded blue rectangle shows the Fermi energy range of our interest around the Dirac band's gap.

[1]Department of Condensed Matter Physics and Materials Science, Tata Institute of Fundamental Research, Homi Bhabha Road, Mumbai 400005, India. [2]Institute of High Performance Computing, Agency for Science, Technology, and Research, Singapore 138632, Singapore. [3]National Institute for Materials Science, 1-1 Namiki, Tsukuba 305-0044, Japan. [4]Division of Physics and Applied Physics, Nanyang Technological University, Singapore 637371, Singapore.
*Corresponding author. Email: deshmukh@tifr.res.in (M.M.D.); biswajitdattaju69@gmail.com (B.D.); justinsong@ntu.edu.sg (J.C.W.S.)

above it. Moreover, we show the continuous variation of Berry's phase–induced quantum oscillation phase shift, as a function of gate voltage (V_{BG}), in an inversion symmetry broken system close to the Dirac band edge. Here, we stress the fact that the Berry's phase of the two bands is not additive (1). It is a routine exercise to map individual Fermi surfaces in a multiband system by isolating different frequencies in SdH oscillations (31), and one can, indeed, measure the Berry's phase of individual bands (26). Together with the fact that in the ABA-trilayer graphene, a well-studied system, one can unambiguously map the band origin of the Landau levels (LLs) using tight binding calculation, our finding that the dependence of one band's quantum oscillation phase on the other is unexpected.

We study a high-mobility (~500,000 cm^2 V^{-1} s^{-1}) hexagonal boron nitride (hBN)–encapsulated ABA-stacked trilayer graphene device (see section S1). A metal top gate and a highly doped silicon back gate ensure independent tunability of charge carrier density and electric field. All the measurements are done with a low-frequency lock-in technique at 1.5 K. The ABA-trilayer graphene is very interesting because it is the simplest system supporting the simultaneous existence of a monolayer graphene (MLG)–like linear and a bilayer graphene (BLG)–like quadratic band in experimentally accessible Fermi energy (see Fig. 1A) (32–37). The structure of the ABA-trilayer graphene

lattice intrinsically breaks the inversion symmetry even at the zero electric field; this generates small mass terms in the Hamiltonian (32, 37). As a result, both pairs of bands are individually gapped as seen in Fig. 1A. Figure 1A shows that when both these bands are filled, the Fermi surface of the ABA-trilayer graphene consists of two Fermi contours—the inner contour comes from the MLG-like band, and the outer contour comes from the BLG-like band. Figure 1B shows that the MLG-like Dirac cone has a robust π Berry's phase, which only reduces to zero in the vicinity of the MLG-like band edge. However, since the Dirac bandgap is very small, ~1 meV (38, 39), it was not possible to resolve the Dirac bandgap and controllably tune the Fermi level through the gap in most of the previous studies (33, 38). Since the LL broadening in our device is small, we can resolve the Dirac bandgap and study the phase of the BLG-like SdH oscillations as the Fermi level is tuned through the MLG-like bandgap. We note that the BLG-like conduction band has more or less a constant trivial Berry's phase 2π in the region of interest (around the Dirac cone gap). In our experiment, we probe a narrow energy window near the MLG-like bandgap. In the following, we use "bandgap" to refer to the MLG-like Dirac bandgap.

In the presence of a magnetic field, the continuous band structure shown in Fig. 1A splits into LLs. The closed orbits $\vec{k}$ space area takes
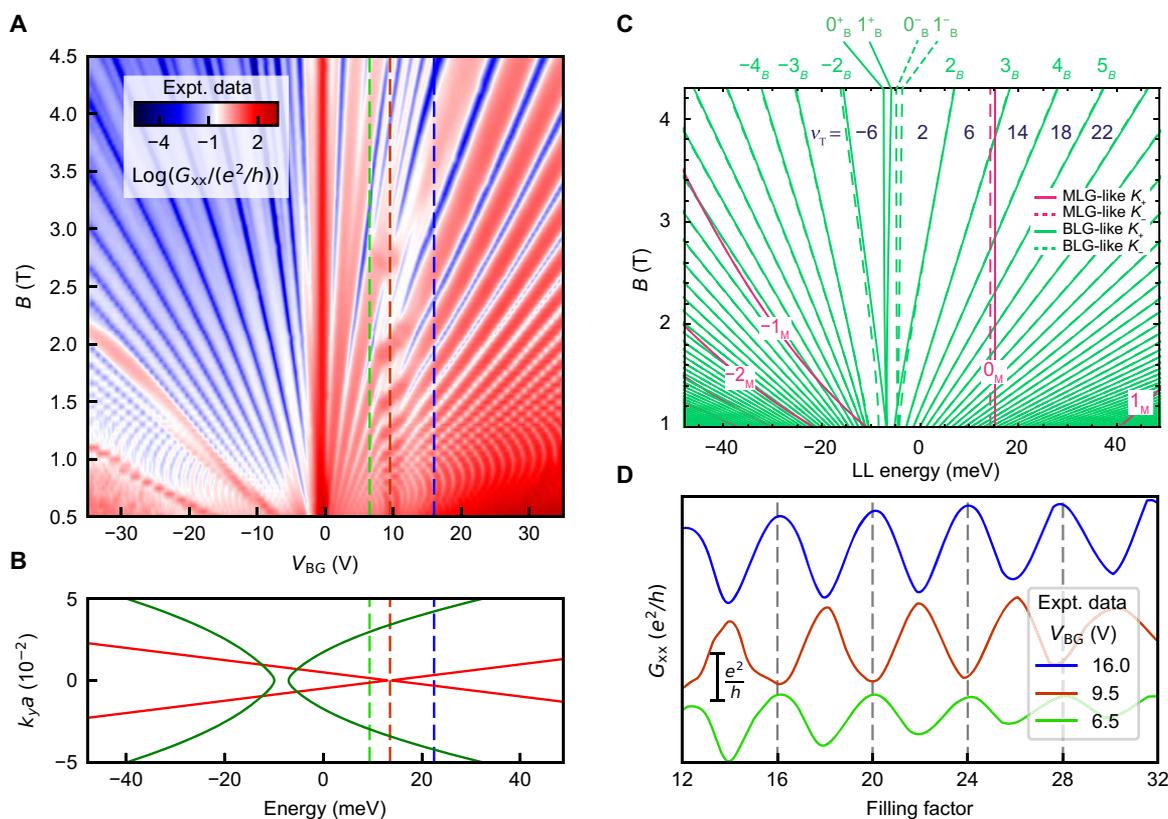

Fig. 2. Quantum oscillation of the ABA-trilayer graphene. (A) Color scale plot of experimentally measured G_{xx} as a function of back gate voltage and magnetic field. The vertical feature parallel to the magnetic field axis at V_{BG}~ 10 V corresponds to the LL crossings of $N_M = 0$ LL with other BLG-like LLs. This V_{BG} also corresponds to the bandgap of the MLG-like bands. (B) Calculated energy band diagram shown in the same energy range as the experimental fan diagram shown in (A). (C) Theoretically calculated LL energies of the spin degenerate LLs as a function of magnetic field. Red and green lines denote LLs originating from the Dirac and the quadratic bands, respectively. Solid and dashed lines denote LLs from K_+ and K_- valleys, respectively. (D) Experimentally measured SdH oscillations (G_{xx}) as a function of filling factor below the bandgap (green), in the bandgap (red), and above the bandgap (blue), which show that the phase of the SdH oscillation in the bandgap is π shifted compared to the other two. The curves are shifted in the vertical direction for clarity. Gate voltage and approximate energy locations of the three SdH oscillation slices are marked with dashed lines of the corresponding color in the fan diagram (A) and in the band structure (B), respectively.

on quantized values that depend on Berry's phase (and magnetic flux). As the magnetic field is swept and the charge density is varied independently, LLs cross the Fermi surface, giving rise to the density of state oscillations that result in longitudinal conductance (G_{xx}) oscillations (40). At a fixed density, the conductance oscillations (SdH) can be written as $\Delta G_{xx} = G \cos \left[2\pi \left(\frac{B_F}{B} + \gamma \right) \right]$, where G is the oscillation magnitude, $B_F = \frac{n_S h}{ge}$ is the SdH oscillation frequency in $1/B$ parameter space, and the phase shift $\gamma = \frac{\Phi_B}{2\pi} - \frac{1}{2}$. Here, n_S is the density in the S sub-band for a multiband system; g is the LL degeneracy, which is four for graphene; and Φ_B is the Berry's phase. Figure 2A shows our measured SdH oscillation in G_{xx} as a function of B and V_{BG}. The corresponding band structure at zero magnetic field is shown in Fig. 2B. Theoretically, calculated LL diagram (Fig. 2C) shows that the MLG-like and the BLG-like LLs disperse as $\sim\sqrt{B}$ and $\sim B$, respectively (32, 34, 37). Details of the tight binding calculation are provided in Materials and Methods and in section S2. The distinct dispersion of the LLs along with the corresponding Hall conductance enables easy identification of the MLG-like and the BLG-like LLs (34, 38, 39, 41).

The central result of our study—that of an unusual phase shift in the quadratic BLG-like band—is vividly illustrated in Fig. 2D. It

shows three slices of BLG-like SdH oscillations at different densities away from the crossing points, which correspond to Fermi levels in the valence band, in the gap, and in the conduction band of the MLG-like Dirac cone, respectively. We emphasize that for all these three densities, the Fermi level lies in the conduction band of the BLG-like band. The SdH oscillations above and below the gap show a π phase shift from the SdH oscillation at the gap. This is intriguing since the BLG-like band in this energy range has a constant trivial Berry's phase (see Fig. 1B). It is clear from the experiment that the Fermi level position in the Dirac band has a bearing on the phase of the BLG-like band. The experimental ability to "tune out" the role of the Dirac band using Fermi energy is crucial to the analysis. It serves as an inbuilt control in our experiment.

We quantify the unusual phase shift via a detailed analysis of the SdH oscillations using the LL index plot (19). Briefly, this involves fitting a line to the LL index (N) corresponding to a minimum in the G_{xx} versus the corresponding inverse magnetic field ($\frac{1}{B}$) plot and examining the intercept at $\frac{1}{B} = 0$. The method of determining LL indices is described in section S2. From the intercept in the LL index axis (Fig. 3A), we see that the intercept is 0.5 (−0.5) in the valence
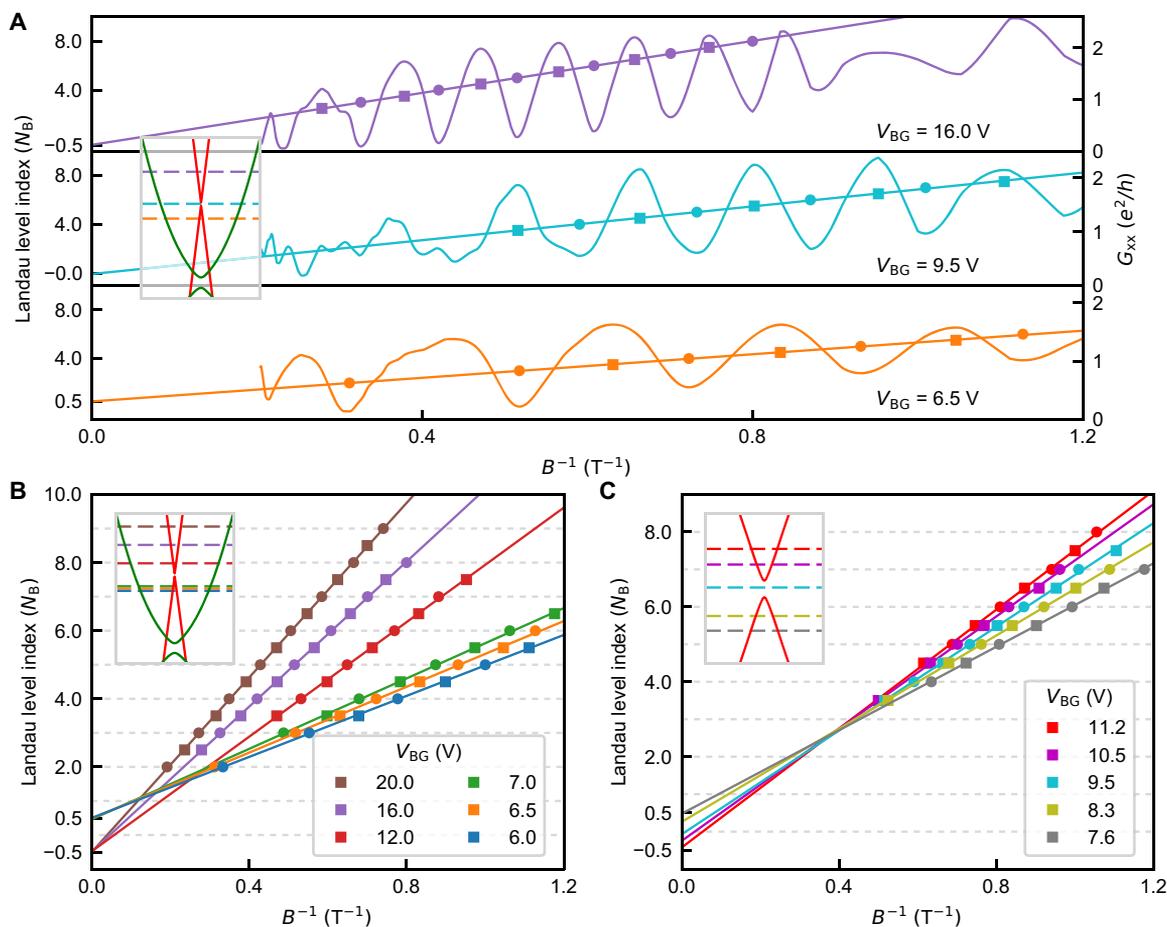

Fig. 3. Unusual SdH phase shift. (A) SdH oscillations (G_{xx}) and the LL index versus inverse magnetic field fit below the bandgap (orange), in the bandgap (cyan), and above the bandgap (purple). Circles and squares denote the SdH minima and maxima, respectively. Inset of all the panels shows the band diagram and the Fermi energy locations for which the SdH fits are shown. (B) LL index versus inverse magnetic field fits at different densities away from the bandgap. The linear fit produces $\pm\frac{1}{2}$ intercept when Fermi level lies in the MLG-like valence band and the MLG-like conduction band, respectively. (C) LL index versus inverse magnetic field fits at different densities close to the bandgap. This shows that the intercept varies continuously from 1/2 to −1/2 when the Fermi level goes from the valence to the conduction MLG-like band by tuning the density. The inset shows the zoomed-in band diagram very close to the bandgap.

(conduction) band and is 0 in the middle of the bandgap. The 0.5 (−0.5) value of the intercept corresponds to a π ($-\pi$) phase shift of the SdH oscillations when the Fermi level lies away from the bandgap even though the phase is extracted only from the BLG-like SdH oscillations. Figure 3B shows fits at several densities away from the gap (firmly in either conduction or valence band). While having different slopes, their intercepts assume only two quantized values: 0.5 or −0.5, depending on the Fermi energy inside the valence or conduction MLG-like Dirac cone. This reinforces the robustness of the unusual phase shift.

Notably, it is only when the Fermi energy is tuned through the MLG-like band's gap that the intercept varies continuously from 0.5 to −0.5 (see Fig. 3C). We note the smooth gate tuning through the bandgap is possible due to the gapless nature of the BLG-like conduction bands throughout the region of interest. Both the nontrivial values and the tunable nature of the unusual phase shift sharply depart from the traditional understanding of quantum oscillation being purely sensitive to the specific Fermi surface it is sampling—BLG-like band in the present case.

We now focus on the origin of the unusual phase shift. In general, SdH oscillations depend on contributions from the Fermi surfaces of both the bands: $\Delta G_{xx} = G_M \cos\left[2\pi\left(\frac{B_{FM}}{B} + \gamma_M\right)\right] + G_B \cos\left[2\pi\left(\frac{B_{FB}}{B} + \gamma_B\right)\right]$, where the M and B subscripts denote MLG-like and BLG-like bands, respectively. As we explain below, the complex pattern of band fillings across multiple bands of distinct type [encoded in (B_{FB}, B_{FM})] controls the SdH oscillations.

To unravel the pattern in the ABA-trilayer graphene, there are two key effects to understand. First, MLG-like LLs have large LL separation (first LL gap is ~50 meV at 2 T) even at small magnetic fields. In contrast, the LL spacing of BLG-like LLs is far smaller (~5 meV at 2 T). This means that multiple BLG-like LLs can be swept through (over large-density and magnetic field windows) while keeping the filling factor of the MLG-like LLs constant in our experiment (see Fig. 2C). This is most prominent between the $N_M = 0$ and $N_M = 1$ MLG-like LLs, where we were able to easily resolve and analyze ~10 BLG-like LLs. Although the filling factor of the BLG-like LLs steadily varies over this region, the filling factor of the MLG-like band remains pinned to 2 due to the particularly large first MLG-like LL energy spacing and the nonmagnetic field dispersive nature of the $N_M = 0$ LL. As a result, in between MLG-like LLs [e.g., that realized in the region $E(0_M) < E_F < E(1_M)$], MLG-like oscillations are frozen, and the SdH oscillations are dominated by the BLG-like band $\Delta G_{xx} \approx G_B \cos\left[2\left(\frac{B_{FB}}{B} + \gamma_B\right)\right]$.

Second, in SdH oscillation measurements, the total density is fixed (set by the gate voltage) while the magnetic field is varied. In the ABA-trilayer graphene, the total density ($n_T = n_M + n_B$) is composed of the individual band densities in each of the MLG-like (n_M) and the BLG-like (n_B) bands, which may reconfigure with the magnetic field while keeping n_T constant. This constraint strongly influences the BLG-like SdH oscillations. To see this, we express its oscillation frequency in terms of the total density via $B_{FB} = \frac{n_B h}{4e} = \frac{(n_T - n_M)h}{4e} = B_{FT} - \frac{\nu_M B}{4}$, where $B_{FT} = \frac{n_T h}{4e}$ and $\nu_M = \frac{n_M h}{eB}$ is the filling
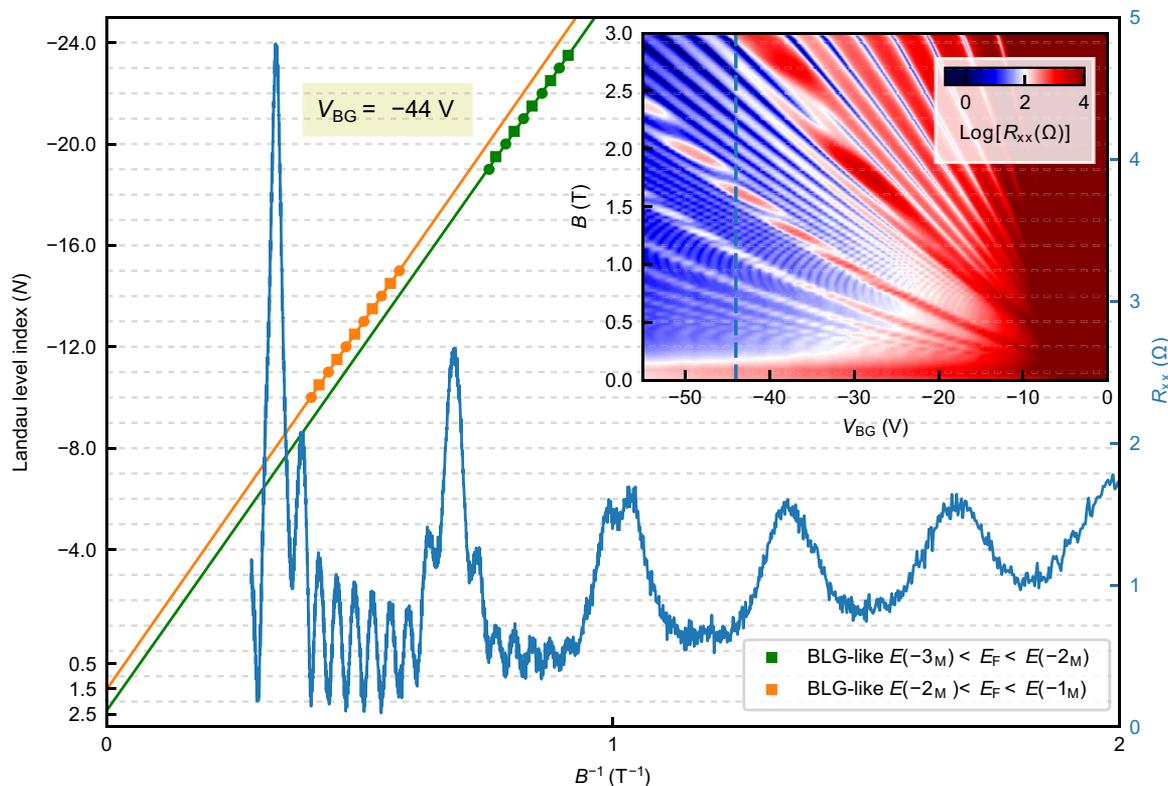

Fig. 4. SdH phase shift when multiple MLG-like LLs are filled. An SdH oscillation line slice of the experimental data showing the beating pattern due to the two bands with different Fermi surface areas. Low- and high-frequency oscillations come from the MLG-like and BLG-like bands, respectively. The LL index plots of BLG-like LLs are shown in orange and green color for which the Fermi energy satisfies $E(-2_M) < E_F < E(-1_M)$ and $E(-3_M) < E_F < E(-2_M)$, respectively. The phases of the BLG-like SdH oscillations in these two regions are shifted differently because of different fillings (of the MLG-like LLs)—this is evident in their different intercepts of 3/2 and 5/2 in the LL index plot. The inset shows the color plot of the resistance on the hole side. The overlaid blue dashed line shows the gate voltage position ($V_{BG} = -44$ V) for which the SdH oscillation is plotted.

factor of the MLG-like band. Crucially, for $E(0_M) < E_F < E(1_M)$ (above the MLG-like bandgap), only $N_M = 0$ electron-like LL is filled, so the filling factor of the MLG-like band remains pinned to 2. This yields a BLG-like oscillation frequency as $\frac{B_{FB}}{B} = \frac{B_{FT}}{B} - 1/2$. Similarly, for $E(-1_M) < E_F < E(0_M)$ (below the MLG-like bandgap), the filling factor of the MLG-like band remains pinned to -2, producing $\frac{B_{FB}}{B} = \frac{B_{FT}}{B} + 1/2$. Incorporating both cases into the BLG-like SdH oscillations, we obtain

$$\Delta G_{xx} \approx G_B \cos\left[2\pi\left(\frac{B_{FT}}{B} + \gamma_B \pm 1/2\right)\right] \qquad (1)$$

that displays an unusual, nontrivial, and tunable phase shift acquired due to the strong filling-enforced constraint above and below the bandgap. This yields an additional π ($-\pi$) phase shift in the BLG-like oscillations due to the fully emptied (fully filled) MLG-like lowest $N_M = 0$ LL. We note that when the Fermi energy is in the bandgap, there is no additional phase shift in the BLG-like band; this is consistent with the expectation that a completely filled (MLG-like valence) band does not influence the transport. We have also extracted this phase from the theoretically calculated density of states, which supports our experimental finding (see section S3).

The filling-enforced constraint is general and should be applicable to higher MLG-like LLs beyond $\nu_M = \pm 2$ discussed above. For example, when the Fermi energy is tuned in between N_M and $(N + 1)_M$ LLs, the MLG-like filling factor similarly remains constant and is pinned to $\nu_M = 4(N_M \pm 0.5)$. Here, $\pm$ refers to the electron (hole)–like LLs. Following the arguments presented before, the BLG-like SdH oscillations in between two MLG-like LLs can be captured by

$$\Delta G_{xx} \approx G_B \cos\left[2\pi\left(\frac{B_{FT}}{B} + \gamma_B - \frac{\nu_M}{4}\right)\right] \qquad (2)$$

As a result, in this region, we expect the BLG-like SdH oscillations to acquire an additional unusual phase $\pi\nu_M/2$ as shown in Eq. 2.

To confirm this, we extracted the SdH phase shift at higher MLG-like LL fillings (see Fig. 4). As shown, when density is tuned to be in the middle of the higher MLG-like LLs with $\nu_M = -6$, the phase shift jumps to 3π (orange) [intercept 3/2]. When density is further tuned so that filling in the MLG-like band is pinned at $\nu_M = -10$, the phase shift reads 5π (green) [intercept 5/2]. This is in clear agreement with Eq. 2. The fact that these higher (odd) phases can be accessed and tuned via gate voltage illustrates the unusual nature
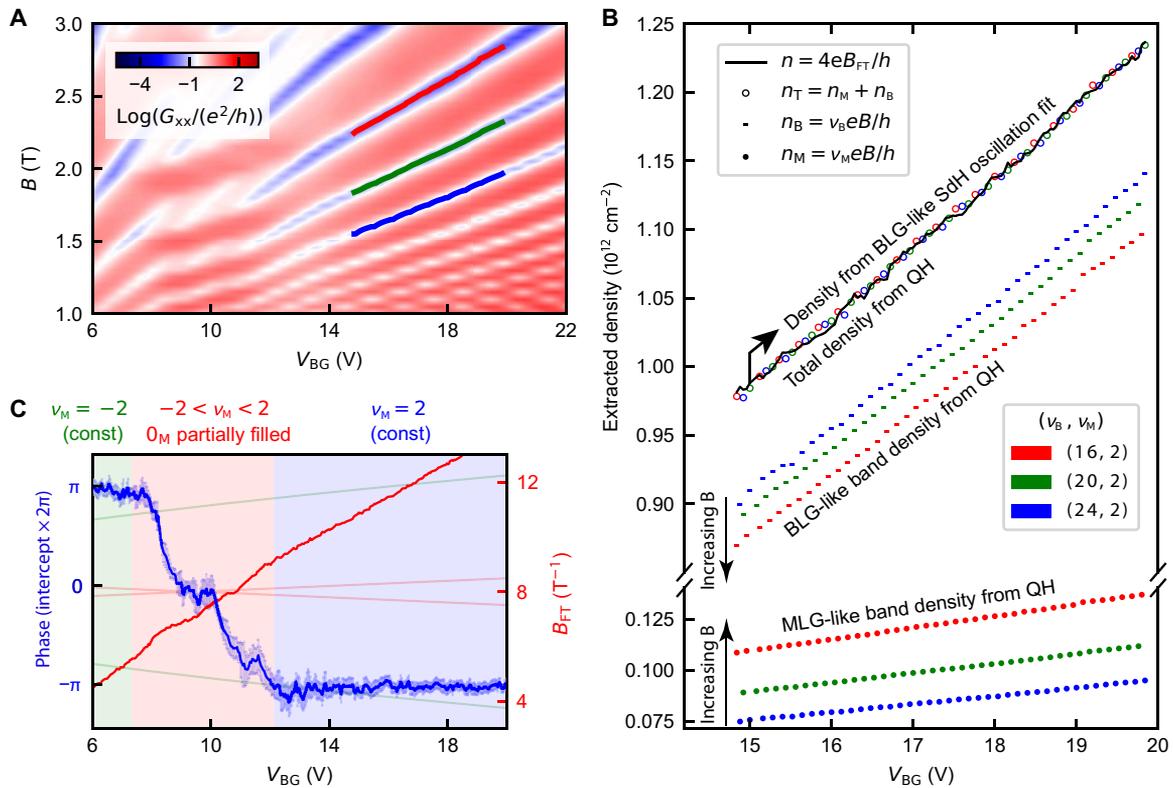

Fig. 5. Consequence of the filling-enforced constraint on SdH frequency and phase. (**A**) Zoomed-in measured LL fan diagram showing three lines drawn for three filling factors, along which we extract the density. (**B**) MLG-like band density ($n_M = \nu_M eB/h$) and BLG-like band density ($n_B = \nu_B eB/h$) calculated from the quantum Hall (QH) data are marked with filled circle and dash, respectively, for total filling factor $\nu_T = 18$ (red), 22 (green), and 26 (blue). The unfilled circles of corresponding colors show the total density $n_T = n_M + n_B$ for each total filling factors. At a constant gate voltage with the increasing magnetic field, the density of the MLG (BLG)–like band increases (decreases), keeping total density constant at all magnetic fields (filling factors). The black line shows the density calculated from the SdH frequency ($n_T = \frac{4e}{h} \times B_{FT}$) of the BLG-like SdH oscillations, which is remarkably close to the combined density calculated from the quantum Hall data for all filling factors. (**C**) Intercept (blue) and slope (red) of the BLG-like SdH oscillation fit as a function of V_{BG}. Fitting errors are shown for the intercept. Corresponding band diagram is overlaid for visualization. Three regions are shaded with three different colors: Green shade and blue shade indicate completely empty and completely filled $N_M = 0$ LL, respectively, whereas the saffron shade indicates partially filled $N_M = 0$ LL.

of the anomalous phase shift and its "filling-enforced" origin (see section S4 for more details).

The filling-enforced constraint is further corroborated by the measured quantum oscillation frequency. In particular, Eq. 1 indicates that the BLG-like quantum oscillations have $1/B$ frequency that scales with the combined density of the MLG-like and the BLG-like bands rather than the density of the BLG-like band only. To illustrate this, we focus on the solid lines in Fig. 5A, where the filling factor takes on precise quantized values $\nu_B = 16,20,24$ with $\nu_M = 2$, obtained directly from Hall conductance measurements (section S2). Hence, using $n_{M(B)} = \nu_{M(B)}eB/h$, as plotted in Fig. 5B, we can calculate the MLG-like band density (colored filled circles) and the BLG-like band density (colored dash plots) on these lines. Total electron density $n_T = n_M + n_B$, which is independent of the filling factor at a given gate voltage, is shown by colored unfilled circles and matches exactly with the density obtained from the oscillation frequency B_F (solid black line in Fig. 5B).

This unprecedented concordance, expected directly from Eq. 1, has a far-reaching consequence—it is assumed that quantum oscillations allow one to isolate a Fermi surface in a multiband system. So, using frequency to isolate the motion of electrons on Fermi surfaces is the de facto method for mapping the Fermi surface. Our analysis shows that for a certain band structure, this simple picture gets modified—in our case, the SdH frequency of the BLG-like band not only depends on the BLG-like band Fermi surface area but also on the MLG-like band Fermi surface area. This, together with the unusual phase shift, unequivocally displays the strong effect of the filling-enforced constraint present in a multiband system.

DISCUSSION

The unusual (nontrivial) zeroth LL filling–enforced phase shifts that we find in the BLG-like bands can be attributed to the Berry's phase of the MLG-like Dirac band, since the existence of the half-filled zeroth LL in a Dirac band is a direct consequence of its nontrivial Berry's phase. We extracted the phase shift (of the BLG-like quantum oscillations) over a fine grid as gate voltage is tuned through the bandgap (see Fig. 5C). This displays the smooth evolution of phase shift from $\pi \rightarrow 0 \rightarrow -\pi$ that closely tracks the smooth evolution of the Berry's phase seen in Fig. 1B expected for the gapped MLG-like band in an inversion symmetry broken ABA-trilayer graphene. This method of phase detection of a nontrivial band using quantum oscillations from a coexisting band with more oscillations is novel; it can provide unexpected new facility to probe nontrivial quantum geometry. The existence of this filling-enforced phase is generically applicable to any multiband system—the unique band structure of the ABA-trilayer graphene, the gate tunability, and the high sample quality just enable this vivid visualization. While our study shows that additional care should be taken to extract the Berry's phase and the Fermi surface area in a multiband system, it could shed light also on other topological materials like Weyl semimetals (42) that host multiple bands.

MATERIALS AND METHODS
Device fabrication
We used the polypropylene carbonate polymer–based dry method to make the hBN–trilayer graphene–hBN stack (43). Electron beam (e-beam) lithography was used to design the electrodes. Argon-oxygen (1:1 ratio) plasma etching was used to define the one-dimensional electrical contacts followed by metal deposition (3-nm chromium,

15-nm palladium, and 30-nm gold) (44). To design a top gate, we transferred one more layer of hBN as the gate insulator. The final step of the e-beam lithography was performed to design the metal top gate.

Numerical simulations
Following the previous theoretical study (32), we numerically calculated the LL energy diagram. We considered the full-tight binding Hamiltonian of the ABA-trilayer graphene (32) with all the hopping parameters. Below are the band parameters we have used for all calculations: $\gamma_0 = 3.1$ eV, $\gamma_1 = 390$ meV, $\gamma_2 = -20$ meV, $\gamma_3 = 315$ meV, $\gamma_4 = 120$ meV, $\gamma_5 = 18$ meV, $\delta = 20$ meV, and $\Delta_2 = 4.3$ meV, which were calculated by matching the experimental LL crossing points with theory. The details of the band parameters' determination and the details of the numerical calculation are described in our earlier study (39).

SUPPLEMENTARY MATERIALS

REFERENCES AND NOTES
1. D. Xiao, M.-C. Chang, Q. Niu, Berry phase effects on electronic properties. *Rev. Mod. Phys.* **82**, 1959–2007 (2010).
2. J. G. Analytis, R. D. McDonald, S. C. Riggs, J.-H. Chu, G. Boebinger, I. R. Fisher, Two-dimensional surface state in the quantum limit of a topological insulator. *Nat. Phys.* **6**, 960–964 (2010).
3. G. P. Mikitik, Y. V. Sharlai, Manifestation of Berry's phase in metal physics. *Phys. Rev. Lett.* **82**, 2147–2150 (1999).
4. A. Alexandradinata, C. Wang, W. Duan, L. Glazman, Revealing the topology of Fermi-surface wave functions from magnetic quantum oscillations. *Phys. Rev. X* **8**, 011027 (2018).
5. S. Mühlbauer, B. Binz, F. Jonietz, C. Pfleiderer, A. Rosch, A. Neubauer, R. Georgii, P. Böni, Skyrmion lattice in a chiral magnet. *Science* **323**, 915–919 (2009).
6. N. Nagaosa, Y. Tokura, Topological properties and dynamics of magnetic skyrmions. *Nat. Nanotechnol.* **8**, 899–911 (2013).
7. B. A. Bernevig, T. L. Hughes, *Topological Insulators and Topological Superconductors* (Princeton Univ. Press, 2013).
8. N. H. Lindner, G. Refael, V. Galitski, Floquet topological insulator in semiconductor quantum wells. *Nat. Phys.* **7**, 490–495 (2011).
9. D. Xiao, W. Yao, Q. Niu, Valley-contrasting physics in graphene: Magnetic moment and topological transport. *Phys. Rev. Lett.* **99**, 236809 (2007).
10. J. Lee, Z. Wang, H. Xie, K. F. Mak, J. Shan, Valley magnetoelectricity in single-layer MoS₂. *Nat. Mater.* **16**, 887–891 (2017).
11. S. Ryu, Y. Hatsugai, Topological origin of zero-energy edge states in particle-hole symmetric systems. *Phys. Rev. Lett.* **89**, 077002 (2002).
12. S. Pancharatnam, Generalized theory of interference, and its applications–Part I. Coherent pencils. *Proc. Indian Acad. Sci. A.* **44**, 247–252 (1956).
13. M. V. Berry, Quantal phase factors accompanying adiabatic changes. *Proc. R. Soc. Lond. A* **392**, 45–57 (1984).
14. I. A. Luk'yanchuk, Y. Kopelevich, Phase analysis of quantum oscillations in graphite. *Phys. Rev. Lett.* **93**, 166402 (2004).
15. F. D. M. Haldane, Berry curvature on the fermi surface: Anomalous Hall effect as a topological fermi-liquid property. *Phys. Rev. Lett.* **93**, 206602 (2004).

16. N. Nagaosa, J. Sinova, S. Onoda, A. H. MacDonald, N. P. Ong, Anomalous Hall effect. *Rev. Mod. Phys.* **82**, 1539–1592 (2010).

17. T. Ando, T. Nakanishi, R. Saito, Berry's phase and absence of back scattering in carbon nanotubes. *J. Physical Soc. Japan* **67**, 2857–2862 (1998).

18. K. S. Novoselov, A. K. Geim, S. V. Morozov, D. Jiang, M. I. Katsnelson, I. V. Grigorieva, S. V. Dubonos, A. A. Firsov, Two-dimensional gas of massless Dirac fermions in graphene. *Nature* **438**, 197–200 (2005).

19. Y. Zhang, Y.-W. Tan, H. L. Stormer, P. Kim, Experimental observation of the quantum Hall effect and Berry's phase in graphene. *Nature* **438**, 201–204 (2005).

20. M. Koshino, E. McCann, Trigonal warping and Berry's phase N π in abc-stacked multilayer graphene. *Phys. Rev. B* **80**, 165409 (2009).

21. L. Zhang, Y. Zhang, J. Camacho, M. Khodas, I. Zaliznyak, The experimental observation of quantum Hall effect of *l*=3 chiral quasiparticles in trilayer graphene. *Nat. Phys.* **7**, 953–957 (2011).

22. B. Büttner, C. X. Liu, G. Tkachov, E. G. Novik, C. Brüne, H. Buhmann, E. M. Hankiewicz, P. Recher, B. Trauzettel, S. C. Zhang, L. W. Molenkamp, Single valley Dirac fermions in zero-gap HgTe quantum wells. *Nat. Phys.* **7**, 418–422 (2011).

23. K. S. Novoselov, E. McCann, S. V. Morozov, V. I. Fal'ko, M. I. Katsnelson, U. Zeitler, D. Jiang, F. Schedin, A. K. Geim, Unconventional quantum Hall effect and Berry's phase of 2π in bilayer graphene. *Nat. Phys.* **2**, 177–180 (2006).

24. C.-H. Park, N. Marzari, Berry phase and pseudospin winding number in bilayer graphene. *Phys. Rev. B* **84**, 205440 (2011).

25. G. P. Mikitik, Y. V. Sharlai, Electron energy spectrum and the Berry phase in a graphite bilayer. *Phys. Rev. B* **77**, 113407 (2008).

26. H. Murakawa, M. Bahramy, M. Tokunaga, Y. Kohama, C. Bell, Y. Kaneko, N. Nagaosa, H. Y. Hwang, Y. Tokura, Detection of Berry's phase in a bulk rashba semiconductor. *Science* **342**, 1490–1493 (2013).

27. P. Wang, B. Cheng, O. Martynov, T. Miao, L. Jing, T. Taniguchi, K. Watanabe, V. Aji, C. N. Lau, M. Bockrath, Topological winding number change and broken inversion symmetry in a Hofstadter's butterfly. *Nano Lett.* **15**, 6395–6399 (2015).

28. R. Akiyama, Y. Takano, Y. Endo, S. Ichinokura, R. Nakanishi, K. Nomura, S. Hasegawa, Berry phase shift from 2π to π in bilayer graphene by Li-intercalation and sequential desorption. *Appl. Phys. Lett.* **110**, 233106 (2017).

29. F. Ghahari, D. Walkup, C. Gutíerrez, J. F. Rodriguez-Nieva, Y. Zhao, J. Wyrick, F. D. Natterer, W. G. Cullen, K. Watanabe, T. Taniguchi, L. S. Levitov, N. B. Zhitenev, J. A. Stroscio, An on/off Berry phase switch in circular graphene resonators. *Science* **356**, 845–849 (2017).

30. J. C. Rode, D. Smirnov, H. Schmidt, R. J. Haug, Berry phase transition in twisted bilayer graphene. *2D Materials* **3**, 035005 (2016).

31. P. J. W. Moll, N. L. Nair, T. Helm, A. C. Potter, I. Kimchi, A. Vishwanath, J. G. Analytis, Transport evidence for Fermi-arc-mediated chirality transfer in the Dirac semimetal Cd₃As₂. *Nature* **535**, 266–270 (2016).

32. M. Serbyn, D. A. Abanin, New dirac points and multiple Landau level crossings in biased trilayer graphene. *Phys. Rev. B* **87**, 115422 (2013).

33. T. Taychatanapat, K. Watanabe, T. Taniguchi, P. Jarillo-Herrero, Quantum Hall effect and Landau-level crossing of Dirac fermions in trilayer graphene. *Nat. Phys.* **7**, 621–625 (2011).

34. B. Datta, S. Dey, A. Samanta, H. Agarwal, A. Borah, K. Watanabe, T. Taniguchi, R. Sensarma, M. M. Deshmukh, Strong electronic interaction and multiple quantum Hall ferromagnetic phases in trilayer graphene. *Nat. Commun.* **8**, 14518 (2017).

35. Y. Shimazaki, T. Yoshizawa, I. V. Borzenets, K. Wang, X. Liu, K. Watanabe, T. Taniguchi, P. Kim, M. Yamamoto, S. Tarucha, Landau level evolution driven by band hybridization in mirror symmetry broken ABA-stacked trilayer graphene. arXiv:1611.02395 (2016).

36. Y. Asakawa, S. Masubuchi, N. Inoue, S. Morikawa, K. Watanabe, T. Taniguchi, T. Machida, Intersubband Landau level couplings induced by in-plane magnetic fields in trilayer graphene. *Phys. Rev Lett.* **119**, 186802 (2017).

37. M. Koshino, E. McCann, Landau level spectra and the quantum Hall effect of multilayer graphene. *Phys. Rev. B* **83**, 165443 (2011).

38. L. C. Campos, T. Taychatanapat, M. Serbyn, K. Surakitbovorn, K. Watanabe, T. Taniguchi, D. A. Abanin, P. Jarillo-Herrero, "Landau level splittings, phase transitions, and nonuniform charge distribution in trilayer graphene." *Phys. Rev. Lett.* **117**, 066601 (2016).

39. B. Datta, H. Agarwal, A. Samanta, A. Ratnakar, K. Watanabe, T. Taniguchi, R. Sensarma, M. M. Deshmukh, Landau level diagram and the continuous rotational symmetry breaking in trilayer graphene. *Phys. Rev. Lett.* **121**, 056801 (2018).

40. A. Isihara, L. Smrcka, Density and magnetic field dependences of the conductivity of two-dimensional electron systems. *J. Phys. C Solid State Phys. Ther.* **19**, 6777 (1986).

41. P. Stepanov, Y. Barlas, T. Espiritu, S. Che, K. Watanabe, T. Taniguchi, D. Smirnov, C. N. Lau, Tunable symmetries of integer and fractional quantum Hall phases in heterostructures with multiple Dirac bands. *Phys. Rev. Lett.* **117**, 076807 (2016).

42. C. M. Wang, H.-Z. Lu, S.-Q. Shen, Anomalous phase shift of quantum oscillations in 3d topological semimetals. *Phys. Rev. Lett.* **117**, 077201 (2016).

43. C. R. Dean, A. F. Young, I. Meric, C. Lee, L. Wang, S. Sorgenfrei, K. Watanabe, T. Taniguchi, P. Kim, K. L. Shepard, J. Hone, Boron nitride substrates for high-quality graphene electronics. *Nat. Nanotechnol.* **5**, 722–726 (2010).

44. L. Wang, I. Meric, P. Y. Huang, Q. Gao, Y. Gao, H. Tran, T. Taniguchi, K. Watanabe, L. M. Campos, D. A. Muller, J. Guo, P. Kim, J. Hone, K. L. Shepard, C. R. Dean, One-dimensional electrical contact to a two-dimensional material. *Science* **342**, 614–617 (2013).

Citation: B. Datta, P. C. Adak, L.-. Shi, K. Watanabe, T. Taniguchi, J. C. W. Song, M. M. Deshmukh, Nontrivial quantum oscillation geometric phase shift in a trivial band. *Sci. Adv.* **5**, eaax6550 (2019).

Science Advances

Nontrivial quantum oscillation geometric phase shift in a trivial band

Biswajit Datta, Pratap Chandra Adak, Li-kun Shi, Kenji Watanabe, Takashi Taniguchi, Justin C. W. Song and Mandar M. Deshmukh

ARTICLE TOOLS	http://advances.sciencemag.org/content/5/10/eaax6550
SUPPLEMENTARY MATERIALS	http://advances.sciencemag.org/content/suppl/2019/10/10/5.10.eaax6550.DC1
REFERENCES	This article cites 42 articles, 4 of which you can access for free http://advances.sciencemag.org/content/5/10/eaax6550#BIBL
PERMISSIONS	http://www.sciencemag.org/help/reprints-and-permissions

Use of this article is subject to the Terms of Service